

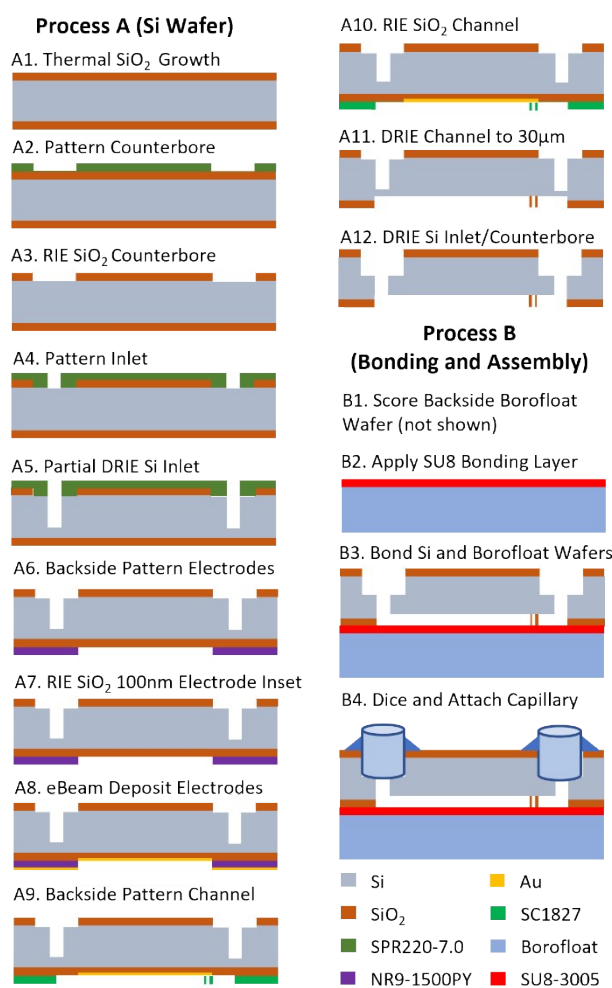
Supplementary Information

Cell Processing Device Fabrication

The cell processing device fabrication sequence can be seen in Supplementary Figure 1. Process A begins with thermal wet oxidation at 1,100 °C of a 4" diameter double side polished p-type <100> orientation silicon wafer (1–20Ω-cm; Polishing Corp of America, Santa Clara, CA) (Figure S1A1). This results in a 3 μm thick silicon dioxide layer on both sides of the wafer that is used as an etchant mask for later silicon etching steps. SPR220-7.0 positive photoresist (PR) (Kayaku Advanced Materials, Westborough, MA) is then spin coated as a photolithography layer on the top of the wafer and 360 μm holes are patterned into the SPR220 with darkfield photolithography (Figure S1A2); these holes serve as counterbores for direct integration of 360 μm OD capillary inlet/outlet connections. The SPR220 layer is deposited by spinning at 750 rpm with a 1.5 second ramp for 5 seconds immediately followed by 2,500 rpm with a 1.5 second ramp for 40 seconds to deposit an approximately 8 μm thick layer. After spin coating, a 3-minute soft bake on a hotplate at 110 °C is followed by darkfield exposure of the desired pattern at 405 nm wavelength and a dosage of 500 mJ/cm². The wafer is held for 5 minutes before developing in MicroPosit MF-319 (Kayaku Advanced Materials, Westborough, MA) for approximately 2 minutes. Following a post exposure bake at 100 °C for 15 minutes, the counterbore pattern is etched through the silicon dioxide layer using a CHF₃ reactive-ion etch (RIE) (Figure S1A3); the remaining SPR220 layer is stripped away with acetone and the wafer is cleaned using an acetone, methanol, isopropanol (AMI) rinse. A new layer of SPR220 is deposited and 100 μm diameter holes are patterned concentric to the counterbore holes. These holes are etched to a depth of approximately 375 μm via a deep reactive-ion etch (DRIE), specifically the Bosch process, to achieve high aspect ratio holes with vertical sidewalls (Figure S1A5). The SPR220 is processed using the same procedure as above except the post exposure bake is extended to 3 hours to ensure the PR mask is sufficiently set prior to the longer DRIE.

Following an AMI clean, NR9-1500PY negative photoresist (Futurrex, Franklin, NJ) is then spun on the backside of the wafer (opposite side of counterbore/inlet holes) with 3 second ramp to 3000 rpm for 40 seconds followed by a 3 second ramp down. A soft bake for 1 minute on a hotplate at 150 °C is performed prior to exposure of the electrode design backside aligned with the inlet holes using 375 nm wavelength at an exposure dosage of 775 mJ/cm². A 1 minute post exposure bake at 100 °C is performed prior to development in RD6 (Futurrex, Franklin, NJ) for approximately 15 seconds followed by a thorough rinse in deionized water (DI); care was taken to not overexposure/overdevelop the electrode design as the negative resist is used as a lift-off layer (Figure S1A6). The electrode design is then inset 100 nm into the oxide layer using an RIE etch; this maintains planarity of the wafer surface after deposition of the electrodes to ensure successful bonding (Figure S1A7). The electrodes are then deposited via e-beam evaporation (Figure S1A8). A 10 nm titanium layer is first deposited as an adhesion layer for the 90 nm gold layer; both layers are deposited at 1 Å/s. The gold that is deposited on top of the photoresist is then lifted off by soaking the wafer for 10 minutes in an acetone bath followed by a short period of sonication to ensure all gold not in way of the electrodes is fully removed.

MicroPosit SC1827 positive photoresist (Kayaku Advanced Materials, Westborough, MA) is then spun on the backside of the wafer (opposite side of counterbore/inlet holes) with 1.5 second ramp to 1000 rpm for 5 seconds followed by 1.5 second ramp to 3000 rpm for 40 seconds. A soft bake for 1 minute on a hotplate at 115 °C is performed prior to exposure of the channel design aligned with the electrodes using 405 nm wavelength at an exposure dosage of 225 mJ/cm² (Figure S1A9). The wafer is held for five minutes



Supplementary Figure 1. Cell processing device fabrication sequence. Devices are batch fabricated with 32 devices on a 4" wafer; the sequence shown is for a cross-section of a single device. As the electrodes are deposited along the channel sides, they are not shown past step A10; see Figure 2 and Figure 5 for alternative views of the device.

following the exposure and then developed in MF-319 for approximately 40 seconds. A hardbake for at least 15 minutes in an oven at 100 °C sufficiently crosslinks the SC1827 to ensure the cell immobilization feature dimensions are preserved as the channel design is etched through the silicon oxide layer via RIE (Figure S1A10). SC1827 is used as it forms a thinner layer than SPR220 allowing for more precise patterning of the 3 µm cell immobilization features. The spin parameters above yield an approximately 1.5 µm thick layer of SC1827 that corresponds to a 0.5 aspect ratio for the photolithography step compared to an aspect ratio of 3 if SPR220 were used.

Following the channel oxide etch, the SC1827 is removed by soaking in acetone followed by a 45 second descum. The silicon in way of the channel is then etched to a depth of 27 µm (resulting in a 30 µm deep channel) using a DRIE (the selectivity of the DRIE is high enough that etching of the exposed oxide and gold can be neglected for the 30 µm etch) (Figure S1A11). Use of the Bosch process allows for straight sidewalls along the channel and between the cell immobilization features where a 10:1 aspect ratio etch is required. The wafer is then flipped over and the inlet holes are through etched via DRIE (Figure S1A12). The counterbore pattern is simultaneously etched during this process as there is no PR mask and the silicon oxide layer was patterned in step A1. This results in a clog resistant inlet/outlet design consisting of a through hole 100 µm in diameter with an outer 360 µm counterbore recessed approximately 250 µm as seen in Figure 5. Process A is completed by sonicating the wafer in acetone to ensure all holes are fully etched through and cleaning the wafer with an AMI rinse.

The bonding process (Process B) begins by scoring the Borofloat wafer in a wafer dicing machine to create two, 80mm by 24mm rectangles (Figure S1B1). The score is less than 50% of the thickness of the wafer to maintain structural rigidity through the subsequent steps. Following scoring, the Borofloat wafer is soaked in a piranha bath (96% H₂SO₄ and 30% H₂O₂ at 3:1 ratio by volume) heated to 125 °C for 1 hour to ensure the surface is free of contaminants. Both the Borofloat and silicon wafer of Process A are then fully dehydrated in an oven at 110 °C to aid in adhesion of the bonding layer. SU8-3005 (MicroChem, Westborough, MA) is then spun on the unscored surface of the Borofloat wafer at 750 rpm with 1.5 second ramp for 5 seconds, 3000 rpm with 1.5 second ramp for 40 seconds, and 4500 rpm with 1 second ramp for 2 seconds. The wafer is then baked on a hotplate for 150 seconds at 90 °C. After 150 seconds, the hotplate is turned off and allowed to cool to 65 °C with the wafer without removing the wafer to minimize thermally induced stress in the SU8 layer that could result from the mismatch in thermal properties between SU8 and Borofloat.¹ The SU8 is then flood exposed to 250 mJ/cm² at 365 nm wavelength (Figure S1B2); no development or post exposure bake was used. SU8 processing was performed only when the relative humidity was between 30% and 70% to ensure good adhesion of the SU8 layer.²

After exposure, the Borofloat wafer is broken along the scores and the resulting rectangular portions aligned over the process A wafer (SU8 down) to fully cover the channel while allowing the connection pads of the electrodes to remain exposed. After securing the rectangles in place with tape, the wafer stack is bonded in an Obducat NanoImprinter held at 130 °C, 10 bar for 30 minutes (Obducat, Burlingame, CA) (Figure S1B3). By forgoing the post exposure bake and development, the SU8 layer is not fully crosslinked at the beginning of the bonding process. As pressure and temperature are applied, the SU8 is able to partially reflow between the wafers to seal between surface imperfections while becoming cross-linked by the bonding heat.¹ During bonding, the silicon wafer is placed on the bottom to maximize conductive heating by the heated lower chuck as the thermal conductivity of Si is an order of magnitude higher than Borofloat; this also prevents the full Si wafer from overhanging the rectangular portions of Borofloat which would lead to cracking when pressure was applied. Following dicing to separate the devices, fabrication is completed by inserting inlet and outlet capillaries in the counterbores and securing with UV activated epoxy, Dymax 9-3095-GEL, using a Dymax Light Welder PC-3D system (Dymax, Torrington, CT) (Figure S1B4).

Isolation of Electrical Systems

During preliminary tests, the ESI spray was severely unstable when the lysis circuit was connected. Open inspection, bubbles were observed in the ESI emitter; bubbles are a common issue in ESI workflows as they lead to both intermittent flow and spray and may also electrically emitter if the spray voltage is applied upstream of the emitter rather than to its outer surface. After confirming the fluidic system was sealed and the fluid was sufficiently degassed, and no electrolysis occurred between the electrodes of the cell processing device, it was hypothesized that electrolysis was occurring along the fluidic path, suggesting an electrical sink in the system. Without the electrical lysis circuit connected, it was observed that metal portions of the syringe were in contact with syringe pump in certain orientations. Reorienting the syringe/applying electrical tape solved this issue and allowed the syringe (and system as a whole) to electrically float, eliminating observable electrolysis bubbles and enabling stable ESI spray. With the lysis circuit connected, all upstream components were at 0 potential, suggesting a path(s) to ground through the lysis circuit. The lysis circuit was thus isolated via a double pole single throw switch such that, during normal operation, the ESI voltage is applied with both sides of the lysis circuit being electrically isolated. This prevents the lysis circuit from serving as a path to ground for the

ESI voltage during analysis while enabling rapid engagement of the lysis circuit. Upon installation of the switch, the ESI spray displayed excellent stability regardless of where the ESI voltage was applied.

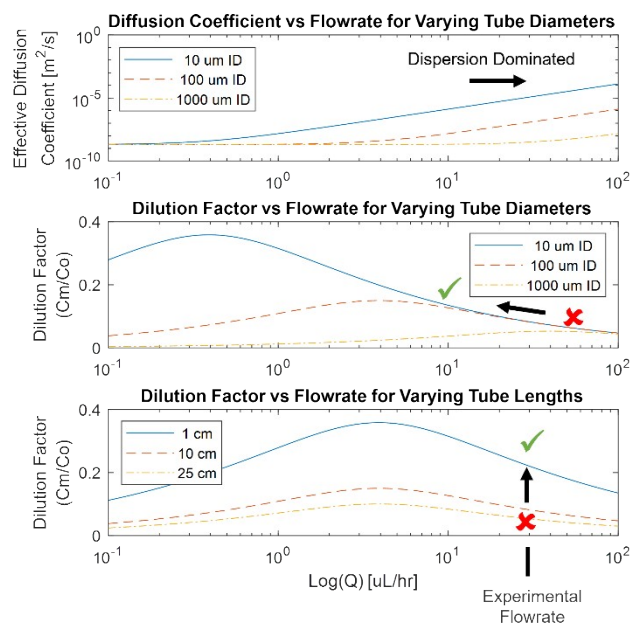
Fluidic System Design and Characterization

Downstream of the cell processing device, diffusive effects must be considered to prevent excessive dilution of the initial lysate volume. As a first approximation, immediately following lysis, the intracellular biomolecules diffuse into the volume of fluid surrounding the cells, forming a lysate band. As the lysate band flows from the cell processing device to the ESI emitter, it undergoes significant band widening. For low Reynold number, high Peclet number flows commonly seen in active flow microfluidic devices, the extent of band widening is dependent on the effective diffusion coefficient resulting from Taylor-Aris dispersion.³

The equivalent Taylor-Aris dispersion coefficient is calculated according to $D_{eff} = D_o (1 + Pe^2/48)$ where the constant in the denominator is dependent on the geometry and is approximated as 48 for incompressible laminar flow of a Newtonian fluid in a constant cross-section pipe (Hagen-Poiseuille flow). The Peclet number is given according to, $Pe = (v * d)/D_o$ where D_o is the molecular weight dependent diffusion coefficient (set as $2 * 10^{-9}$ m²/s to represent metabolites), d is the tube inner diameter, and v is the velocity of the fluid for a given flowrate. The effective diffusivity results in growth of the band according to, $w = 4\sqrt{\ln(2)} \sqrt{D_{eff} * t}$. The mean concentration across the resulting bandwidth can then be determined as $C_m = (C_o w_o)/(w_o + w)$ where C_o is the initial concentration (here taken as 1 for non-dimensional purposes) and w_o is the initial bandwidth.

Dispersion effects were investigated for various flowrate, ID, and length combinations relevant the microfluidic workflow. Assuming a 10 cm length of tubing, the Taylor-Aris effective diffusion coefficient rapidly increases (orders of magnitude higher than the absolute diffusion coefficient) for flowrates exceeding 1 μ L/hr as shown in Supplementary Figure 2 (top). Dispersion becomes the controlling method of dilution in this region. The resulting nondimensional dilution factor (C_m/C_o) is plotted vs flowrate for varying tube diameters (again assuming a 10 cm length of tubing); the dilution curves collapse for microfluidic tube diameters (10-100 μ m ID) at nano-ESI flowrates (1-10 nL/s) (middle). At the experimental flowrate of 30 μ L/hr (8.3 nL/s), the internal diameter has minimal impact on the dilution factor and was selected as 50 μ m to balance a rapid response against constraints of sustainable pressure drop. Solving the dilution factor vs flowrate for a 100 μ m ID tube at varying tube lengths highlights the importance of minimizing tubing length between the cell processing device and the ESI emitter to mitigate dispersion effects. The length of capillary is the controlling parameter with regard to dispersion and must be minimized where possible; minimizing tube length also reduces transit time and pressure drop.

Dispersion modelling also provides useful information as to the delay, duration, and anticipated concentration of analytes in the lysate upon entering the MS. As such, a representative experimental setup was modelled to inform post-processing of MS spectra. Given the low dead volume between the cell immobilization features and device outlet, system modelling began immediately downstream of the device. A 5 cm length of 50 μ m capillary leads to a microvalve with 170 nL volume (dispersion in the valve is not considered). A 2.5 cm, 100 μ m nominal ID ESI emitter is connected to the valve. The initial bandwidth was determined for a packed condition in which the cells accumulate at the channel restriction (assuming a double layer of 15 μ m diameter cells packed 6 abreast in the 100 μ m x 30 μ m channel). The initial dilution upon lysis is given by the intracellular volume divided by the lysate band volume. As the packing density is assumed constant, the initial dilution factor is independent of cell number and equal to approximately 47%. Following dispersion from the lysis location to the emitter, the final dilution factor is approximately 0.4%. Considering a single analyte at an intracellular concentration of 1 μ M, the average concentration in the dispersed lysate band will

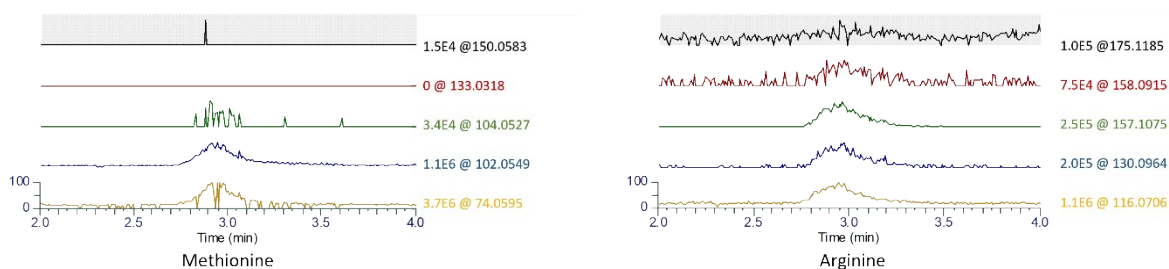


Supplementary Figure 2. Taylor-Aris dispersion modelling informs optimal flowrate, tube diameter, and tube lengths to maintain small concentrations of analytes resulting from the small lysate volume while balancing time and pressure drop considerations. (Top) Plot of effective diffusion coefficient vs flowrate for a 10 cm length of tubing shows that dispersion becomes dominant means of diffusive transport at higher flowrates. (Middle) Plot of mean concentration (normalized C_m/C_o where C_o is initial concentration) vs flowrate for 10 cm length of tubing shows that dilution curves collapse for microfluidic tube diameters (10-100 μ m ID) at nano-ESI flowrates (1-10 nL/s). (Bottom) Plot of mean concentration vs flowrate for varying tube lengths for a 100 μ m ID tube highlights importance of minimizing tube length to mitigate dilution effects. Reducing length also reduces transit time and pressure drop. For reference the experimental flowrate was 30 μ L/hr (8.3 nL/s).

be a mere 4 nM at the emitter tip if extracted from 100 cells. Increasing the number of cells significantly reduces the final dilution (nearly directly proportional), increasing the dilution factor to 4% from 1000 cells. Regardless of cell number, a delay of approximately 55 seconds is expected from the time of lysis to the ESI emitter with the lysate bandwidth corresponding to approximately 20 seconds of spray at a flowrate of 30 $\mu\text{L/hr}$.

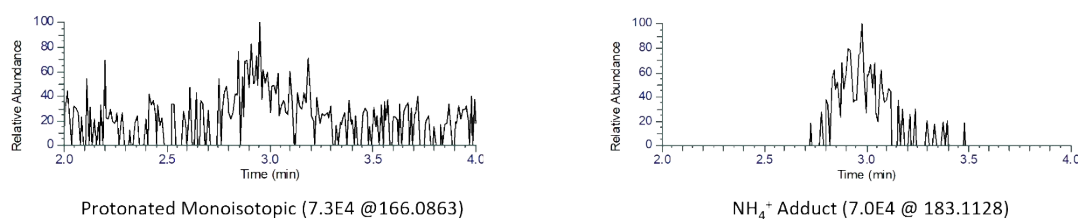
Application to Intracellular Monitoring

Five of the nineteen amino acids displayed no distinct signal increase at the protonated monoisotopic mass following initial analysis. Additional m/z values were investigated based on fragments reported in open-source ESI-MS databases as well as potential adducts (e.g., Na^+ , K^+ , NH_4^+). Both methionine and arginine displayed distinct signal increases for several of the most common fragments reported in the MassBank Europe database.



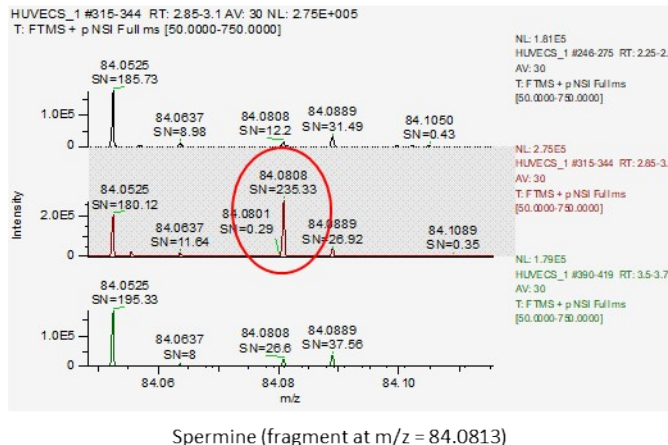
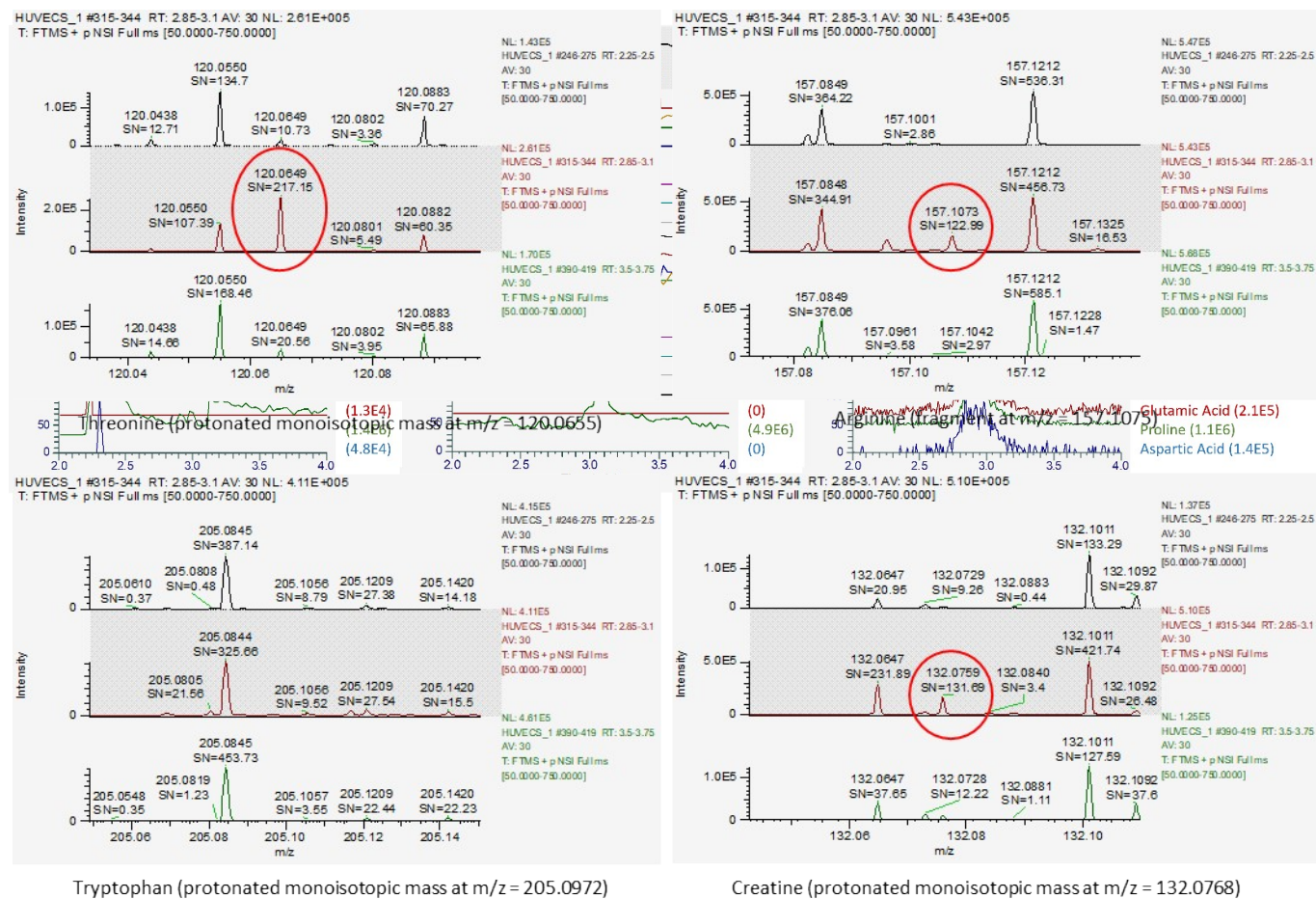
Supplementary Figure 3. Both methionine and arginine show little variation in the protonated monoisotopic mass traces (top trace) but display distinct signal increases in multiple fragments reported in the MassBank Europe database for ESI-MS. The traces are normalized by the maximum signal intensity for the displayed time range; the maximum signal intensity and corresponding mass are provided to the right of each trace.

Though no common fragments were seen for phenylalanine, the NH_4^+ adduct displayed a distinct increase compared to the protonated monoisotopic mass; NH_4^+ is present at high concentration in the buffer.



Supplementary Figure 4. The NH_4^+ adduct of phenylalanine (right) displayed a distinct signal increase compared to the protonated monoisotopic mass trace (left). The traces are normalized by the maximum signal intensity for the displayed time range.

Individual spectra of representative metabolites are included in Supplementary Figure 5. Threonine and creatine were both detected at the protonated monoisotopic mass while arginine and spermine were detected as fragments. Tryptophan was not detected at either the protonated monoisotopic or fragment masses. The sensitivity of the system to cell number was characterized by comparing the number of protonated monoisotopic amino acid masses detected. For 200 cells, the concentration of analytes following dispersion is below the limit of detection as no traces display a clear signal at the anticipated lysate elution time point of approximately 3 minutes. For 500 cells, three of the amino acids were detected compared to fourteen of the nineteen for 1500 cells. Comparison of the amino traces for each cell loading can be seen in Supplementary Figure 6.



Supplementary Figure 5. Representative spectra of both detected and undetected metabolites. For each analyte, the target m/z is shown for time periods before (top), during (middle), and after (bottom) lysate elution; the spectra are averaged over 15 seconds for each time point. Signal to noise (SN) values are provided for each m/z marker with the detected signals circled in red; tryptophan was not detected. The target m/z value is listed below each sub-figure and denoted as either a protonated monoisotopic mass or fragment mass; instrument error was taken as 10 ppm for the analysis.

References

1. Madou, R. M.-D. M. J., SU-8 Photolithography and Its Impact on Microfluidics. In *Microfluidics and Nanofluidics Handbook: Fabrication, Implimentation, and Applications*, Chakraborty, S. K. M. S., Ed. CRC Press: Boca Raton, FL, 2012; pp 231-268.
2. Birleanu, C.; Pustan, M.; Voicu, R.; Serdean, F.; Merie, V., Humidity influence on the adhesion of SU-8 polymer from MEMS applications. *MATEC Web Conf.* **2017**, *137*, 08002.
3. Kirby, B. J., *Micro- and Nanoscale Fluid Mechanics: Transport in Microfluidic Devices*. Cambridge University Press: Cambridge, 2010.